Supporting Information:

Supersonic Microwave Plasma: Potential and Limitations for Energy-Efficient CO_2 Conversion

Vincent Vermeiren* and Annemie Bogaerts

Department of Chemistry, Research group PLASMANT, University of Antwerp, Universiteitsplein 1, 2610 Antwerp, Belgium

1 List of Chemical Reactions Included in the Model

Table S1: Electron impact reactions calculated with cross sections data, using the calculated EEDF, as explained in section 2.3 of the main paper, as well as the references where the data are adopted from.

No.	Reaction	Ref	Note*
(X1)[a]	$e^- + CO_2 \rightarrow 2e^- + CO_2^+$	S1	
(X2)[b]	$e^- + CO_2 \rightarrow 2e^- + O + CO^+$	S1	
(X3)[b]	$e^- + CO_2 \rightarrow O^- + CO$	S1	
(X4)[b]	$e^- + CO_2 \rightarrow e^- + O + CO$	S1	
(X5)[a]	$e^- + CO_2 \rightarrow e^- + CO_2[e_1]$	S1	
(X6)[c]	$e^- + CO_2 \leftrightarrow e^- + CO[v_i]$	S1	i=a,b,c,d
(X7)[c]	$e^- + CO_2[v_i] \leftrightarrow e^- + CO_2[v_j]$	S1	i=0-5
(X8)[b]	$e^- + CO \rightarrow 2e^- + CO^+$	S2	
(X9)[b]	$e^- + CO \rightarrow C + O^-$	S3	
(X9bis)[b]	$e^- + CO \rightarrow e^- + C + O$	S4	
(X10)[a]	$e^- + CO \rightarrow e^- + CO[e_x]$	S4	x=1-4
(X11)[c]	$e^- + CO \rightarrow e^- + CO[v_i]$	S4	i=1-10
(X12)[b]	$e^- + O_2 \rightarrow e^- + O + O$	S5	
(X12M)[a]	$e^- + O_2 + M \rightarrow e^- + O_2^- + M$	S5	
(X13)[b]	$e^- + O_2 \rightarrow O + O^-$	S5	
(X14)[c]	$e^- + O_2 \leftrightarrow e^- + O_2[v_i]$	S5	i=1,2,3
(X15)[a]	$e^- + O_2 \leftrightarrow e^- + O_2[e_x]$	S5	x=1,2

a) Same cross section also used for $CO_2 v_i$ (i = the various vibrationally excited levels)
b) Cross section also used for $CO_2 v_i$, modified by lowering the energy threshold by the energy of the excited state of $CO_2 v_i$
c) Cross section for the various levels (i,j) scaled and shifted using Fridman's approximation from the $(0 \rightarrow 1)$ cross-section
* v_0 is ground state

Table S2: Electron impact reactions using analytical expressions for the rate coefficients, given in m^3/s and m^6/s, for two-body and three-body reactions, respectively, as well as the references where the data are adopted from. T_g and T_e are given in K and eV, respectively.

No.	Reaction	Rate coefficient	Reference
(E1a)	$e^- + CO_2^+ \rightarrow CO(v_1) + O$	$1 \times 10^{-11} T_e^{-0.5} T_g^{-1}$	S6,S7
(E1b)	$e^- + CO_2^+ \rightarrow C + O_2$	$1 \times 10^{-11} T_e^{-0.5} T_g^{-1}$	S8
(E2)[a]	$e^- + CO_4^+ \rightarrow CO_2 + O_2$	$1.61 \times 10^{-13} T_e^{-0.5}$	S8
(E3)	$e^- + CO^+ \rightarrow C + O$	$3.46 \times 10^{-14} T_e^{-0.48}$	S9,S10
(E4)[a]	$e^- + O + M \rightarrow O^- + M$	1×10^{-43}	S7

[a] The primary source was not accessible

Table S3: Ion-ion and ion-neutral reactions, as well as the references where the data are adopted from. The rate coefficients are given in m^3/s and m^6/s, for two-body and three-body reactions, respectively. T_g is given in K.

No.	Reaction	Rate coefficient	Reference
(I1)	$CO_2 + CO^+ \rightarrow CO_2^+ + CO$	1.0×10^{-15}	S11,S12
(I2a)[b]	$CO_2 + O^- + CO_2 \rightarrow CO_3^- + CO_2$	1.5×10^{-40}	S11,S13
(I2b)[b]	$CO_2 + O^- + CO \rightarrow CO_3^- + CO$	1.5×10^{-40}	S11,S13
(I2c)	$CO_2 + O^- + O_2 \rightarrow CO_3^- + O_2$	3.1×10^{-40}	S11,S13
(I3)	$CO_2 + O_2^- + M \rightarrow CO_4^- + M$	4.7×10^{-41}	S11,S13
(I4)	$CO + O^- \rightarrow CO_2 + e$	5.5×10^{-16}	S11,S14
(I5)	$CO + CO_3^- \rightarrow 2CO_2 + e$	5×10^{-19}	S15
(I6)[a]	$CO_3^- + CO_2^+ \rightarrow 2CO_2 v_b + O$	5×10^{-13}	S7
(I7)[a]	$CO_4^- + CO_2^+ \rightarrow 2CO_2 v_b + O_2$	5×10^{-13}	S7
(I8)[a]	$O_2^- + CO_2^+ \rightarrow CO_2 v_1 + O_2 + O$	6×10^{-13}	S7
(I9)	$CO_3^- + O \rightarrow CO_2 + O_2^-$	8×10^{-17}	S16
(I10a)[a]	$CO_4^- + O \rightarrow CO_3^- + O_2$	1.12×10^{-16}	S11
(I10b)[a]	$CO_4^- + O \rightarrow CO_2 + O_2 + O^-$	1.4×10^{-17}	S11
(I11)	$O + O^- \rightarrow O_2 + e$	2.3×10^{-16}	S17
(I12)[a]	$O + O_2^- \rightarrow O_2 + O^-$	1.5×10^{-16}	S11
(I13)	$O_2^- + M \rightarrow O_2 + M + e$	$2.7 \times 10^{-16} (\frac{T_g}{300})^{0.5} exp(-5590/T_g)$	S18,S19
(I14)[c]	$O^- + M \rightarrow O + M + e$	$2.3 \times 10^{-15} exp(-26000/T_g)$	S19–S21

[a] The primary source was not accessible

[b] The rate coefficient of $CO_2 + O^- + He \rightarrow CO_3^- + He$ was used, due to the lack of further information.

[c] For usual values of gas temperature, i.e. $T_g \ll 26000$ K, the rate coefficient is very low, as pointed out by Gudmundsson.[S22]

Table S4: Neutral-neutral reactions, as well as the references where the data are adopted from. The rate coefficients are given in m^3/s and m^6/s, for two-body and three-body reactions, respectively. T_g is given in K. The α parameter determines the effectiveness of lowering the activation energy for reactions involving vibrationally excited levels of the molecules (see details in S23,S24).

No.	Reaction	Rate coefficient	α	References
(N1)	$CO_2 + M \rightarrow CO + O + M$	$6.06 \times 10^{-16} exp(-52525/T_g)$	0.82	S25
(N2)	$CO_2 + O \rightarrow CO + O_2$	$2.8 \times 10^{-17} exp(-16400/T_g)$	0.57	S26
(N3)	$CO_2 + C \rightarrow 2CO$	$< 10^{-21}$	n.a.	S27
(N4)[a]	$CO + O + M \rightarrow CO_2 + M$	$8.3 \times 10^{-46} exp(-1510/T_g)$	0.0	S28,S29
(N5)	$O_2 + CO \rightarrow CO_2 + O$	$4.2 \times 10^{-18} exp(-24000/T_g)$	0.5	S29
(N6)	$O_2 + C \rightarrow CO + O$	$1.99 \times 10^{-16} exp(-2010/T_g)$	0.0	S30
(N7)	$O + C + M \rightarrow CO + M$	$2.14 \times 10^{-41} (\frac{T_g}{300})^{-3.08} exp(-2144/T_g)$	n.a.	S29,S31
(N8)	$O + O + M \rightarrow O_2 + M$	$5.2 \times 10^{-47} exp(900/T_g)$	n.a.	S29,S31
(N9)	$O_2 + M \rightarrow O + O + M$	$3.0 \times 10^{-12} \frac{1}{T_g} exp(-59380/T_g)$	0.0	S29,S31

[a] Multiply by 7, 3 or 12 for M= CO_2, CO or O_2 respectively.

Table S5: Neutral reactions between vibrationally excited molecules, as well as the references where the data are adopted from. The rate coefficients are given in m^3/s and m^6/s, for two-body and three-body reactions, respectively. T_g is given in K.

No.	Reaction	Rate coefficient	References
(V1)	$CO_2 v_a + M \rightarrow CO_2 + M$	$7.14 \times 10^{-15}\, exp(-177\, T_g^{-1/3} + 451\, T_g^{-2/3})$	S32–S34
(V2a)	$CO_2 v_1 + M \rightarrow CO_2 v_a + M$	$4.25 \times 10^{-7}\, exp(-407\, T_g^{-1/3} + 824\, T_g^{-2/3})$	S34–S36
(V2b)	$CO_2 v_1 + M \rightarrow CO_2 v_b + M$	$8.57 \times 10^{-7}\, exp(-404\, T_g^{-1/3} + 1096\, T_g^{-2/3})$	S34–S36
(V2c)	$CO_2 v_1 + M \rightarrow CO_2 v_c + M$	$1.43 \times 10^{-7}\, exp(-252\, T_g^{-1/3} + 685\, T_g^{-2/3})$	S34–S36
(V3)	$CO v_1 + M \rightarrow CO + M$	$1.0 \times 10^{-18}\, T_g\, exp(-150.7\, T_g^{-1/3})$	S37
(V4)	$O_2 v_1 + M \rightarrow O_2 + M$	$1.3 \times 10^{-14}\, exp(-158.7\, T_g^{-1/3})$	S33,S34
(V5)	$CO_2 v_1 + CO_2 \rightarrow CO_2 v_a + CO_2 v_b$	$1.06 \times 10^{-11}\, exp(-242\, T_g^{-1/3} + 633\, T_g^{-2/3})$	S34–S36
(V6)	$CO_2 v_1 + CO_2 \rightarrow CO_2 + CO_2 v_1$	$1.32 \times 10^{-18}\, (\frac{T_g}{300})^{0.5} \frac{250}{T_g}$	S38,S39
(V7)	$CO v_1 + CO \rightarrow CO + CO v_1$	$3.4 \times 10^{-16} (\frac{T_g}{300})^{0.5}\, (1.64 \times 10^{-6}\, T_g + \frac{1.61}{T_g})$	S40,S41
(V8)	$CO_2 v_1 + CO \rightarrow CO_2 + CO v_1$	$4.8 \times 10^{-12}\, exp(-153\, T_g^{-1/3})$	S34,S35

2 Flow Results for an Inlet Pressure of 4 bar

Figure S1 shows the flow results at a higher inlet pressure than presented in the main paper, namely 4 bar, and an outlet pressure of 1 bar. The results show the formation of a third distinct region (III), called the shock train, that forms between the supersonic and the mixing region. The shock train is characterized by a sequence of shocks separating subsonic from supersonic regions.[S42] After each shock, the flow accelerates again to supersonic velocities, after which it is decelerated by the following shock. The region is characterized by pressure and temperature oscillations.

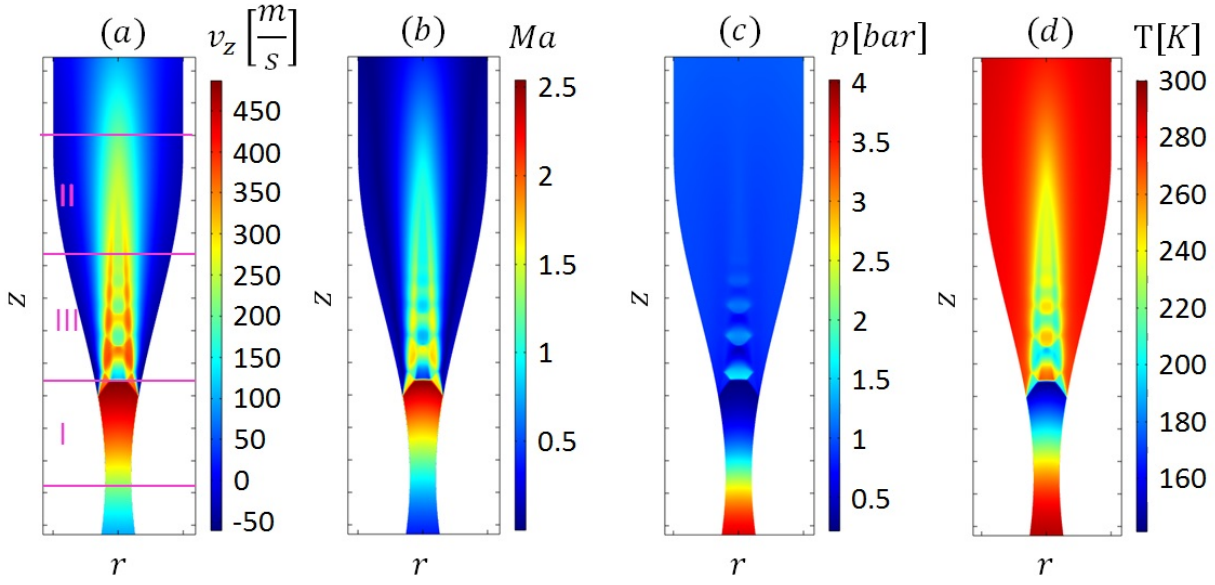

Figure S1: (a) Axial velocity magnitude, (b) Mach number, (c) static pressure and (d) static temperature in the case of $r_1 = 0.4$ cm, $r_2 = 2$ cm, $z_1 = 10$ cm, $p_{in} = 4$ bar, $p_{out} = 1$ bar.

3 Vibrational Energy Transfer

In figure 6 of the main paper, it was shown that in the beginning of the plasma, VV relaxation transports energy from the higher vibrational levels to lower vibrational levels in a ladder downclimbing process. The explanation for this lies in the fact that CO_2(V2) receives more energy from the electrons than CO_2(V1). This can be seen in figure S2, where the rate of

electron energy loss to the lowest vibrational levels upon excitation from ground state CO_2 is shown. Next to the fact that more electron energy goes to the second level of the asymmetric vibrational mode instead of the first level, the density of the latter can be further depleted by electron impact vibrational excitation from that level to the higher vibrational levels.

The VV energy transfer reacts to this non-equilibrium between the first and the second vibrational level. In figure S3, it can be seen that the first vibrational level is strongly populated by VV relaxation.

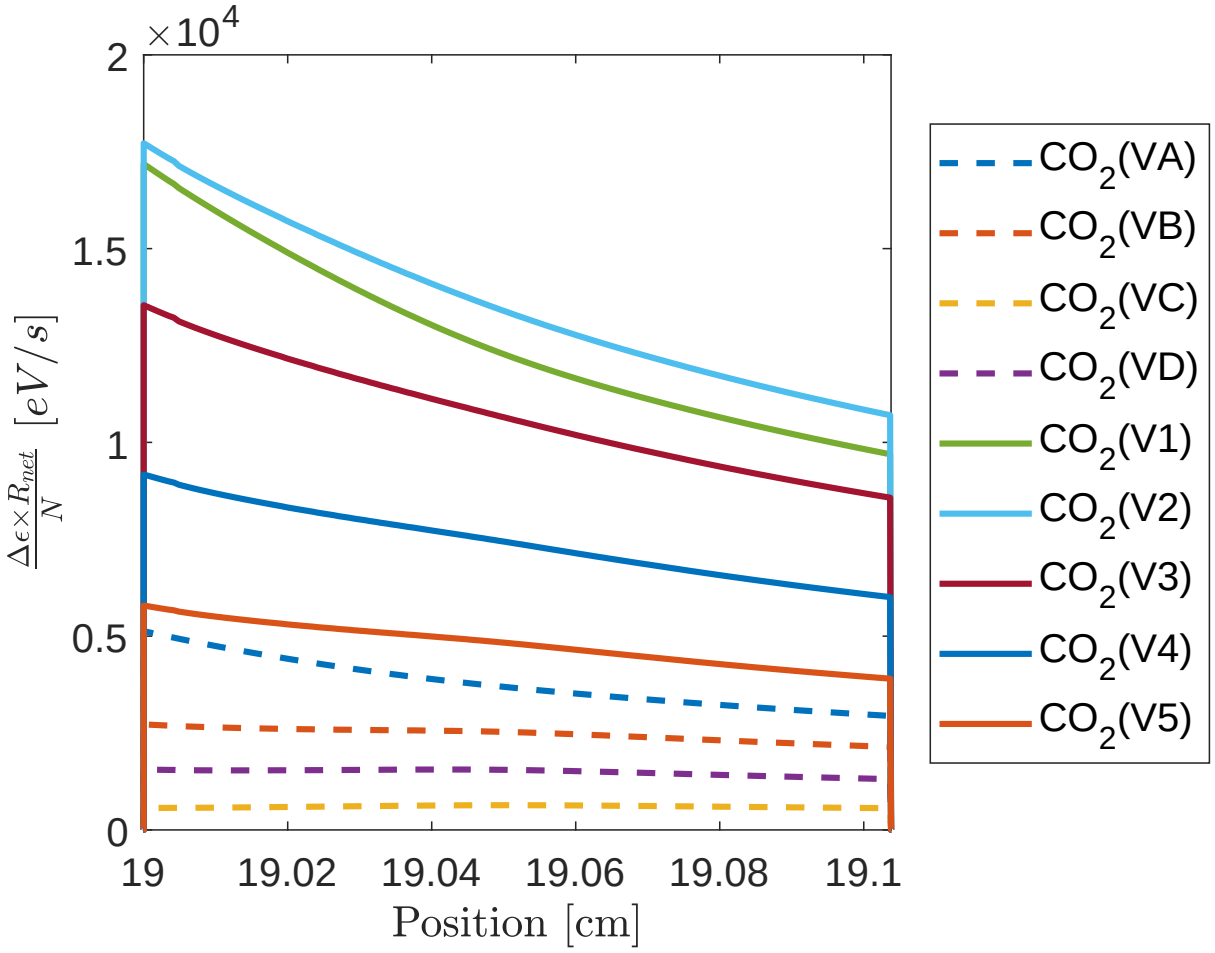

Figure S2: Electron energy loss to the different vibrational levels from ground state CO_2 inside the plasma, which ranges from z=19 to z=19.1 cm (cf. Figure 6 of the main paper), with SEI = 0.2 eV/molec. The other conditions are: $r_1 = 0.4$ cm, $r_2 = 2$ cm, $z_1 = 10$ cm, $p_{in} = 2$ bar, $p_{out} = 1$ bar

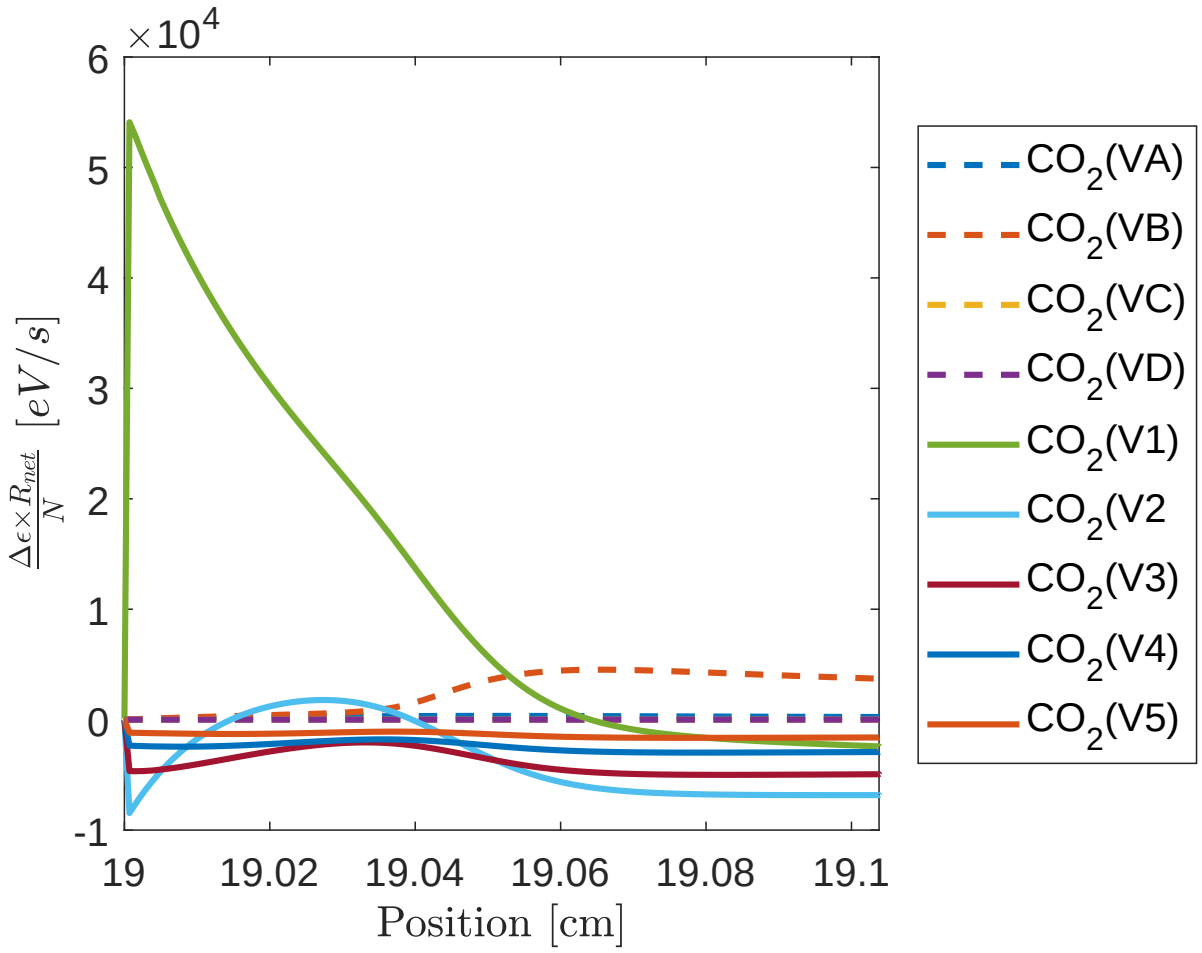

Figure S3: Energy transfer to the different levels in VV relaxation from the other levels, inside the plasma, ranging from z=19 to z=19.1 cm, with SEI = 0.2 eV/molec. The other conditions are: $r_1 = 0.4$ cm, $r_2 = 2$ cm, $z_1 = 10$ cm, $p_{in} = 2$ bar, $p_{out} = 1$ bar.

4 Effect of the Power on the Energy Efficiency

In figure S4 we show the energy efficiency and conversion as a function of the plasma position in the reactor, at three different SEI values, namely 0.05, 0.1, 0.15, and 0.2 eV/molec. The energy efficiency shows the same trend in the four different cases.

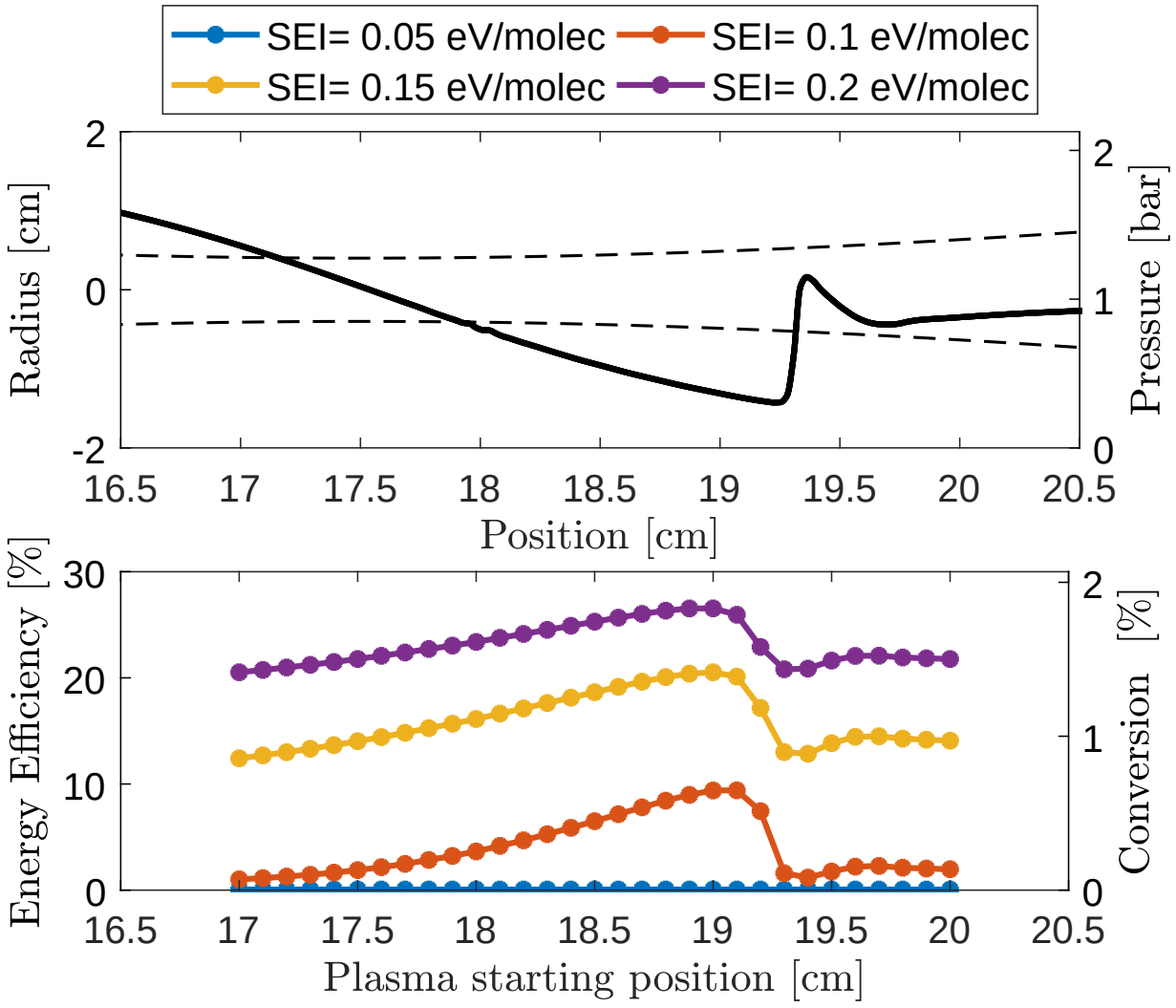

Figure S4: Conversion and energy efficiency (bottom panel) as a function of plasma position in the reactor, for four different SEI values. The other conditions are: $r_1 = 0.4$ cm, $r_2 = 2$ cm, $z_1 = 10$ cm, $p_{in} = 4$ bar, $p_{out} = 1$ bar. The radius of the reactor (dashed line) and pressure (full line) are plotted in the top panel.

5 Flow results for different inlet pressure

Figure S5 shows the evolution of the Mach number (top panel), pressure (middle panel) and temperature (bottom panel) for different inlet pressures, and an outlet pressure of 1 bar. With increasing inlet pressure, the maximum Mach number increases, and the minimum temperature decreases. In addition, the pressure minimum in the supersonic region decreases when the inlet pressure rises from 1.2 bar to 2 bar. A further increase of the inlet pressure does not change the minimum pressure, since the total pressure increases as well, requiring a higher Mach number to reach the same pressure in the supersonic region. The position of the pressure minimum, however, shifts a bit to later in the supersonic reactor.

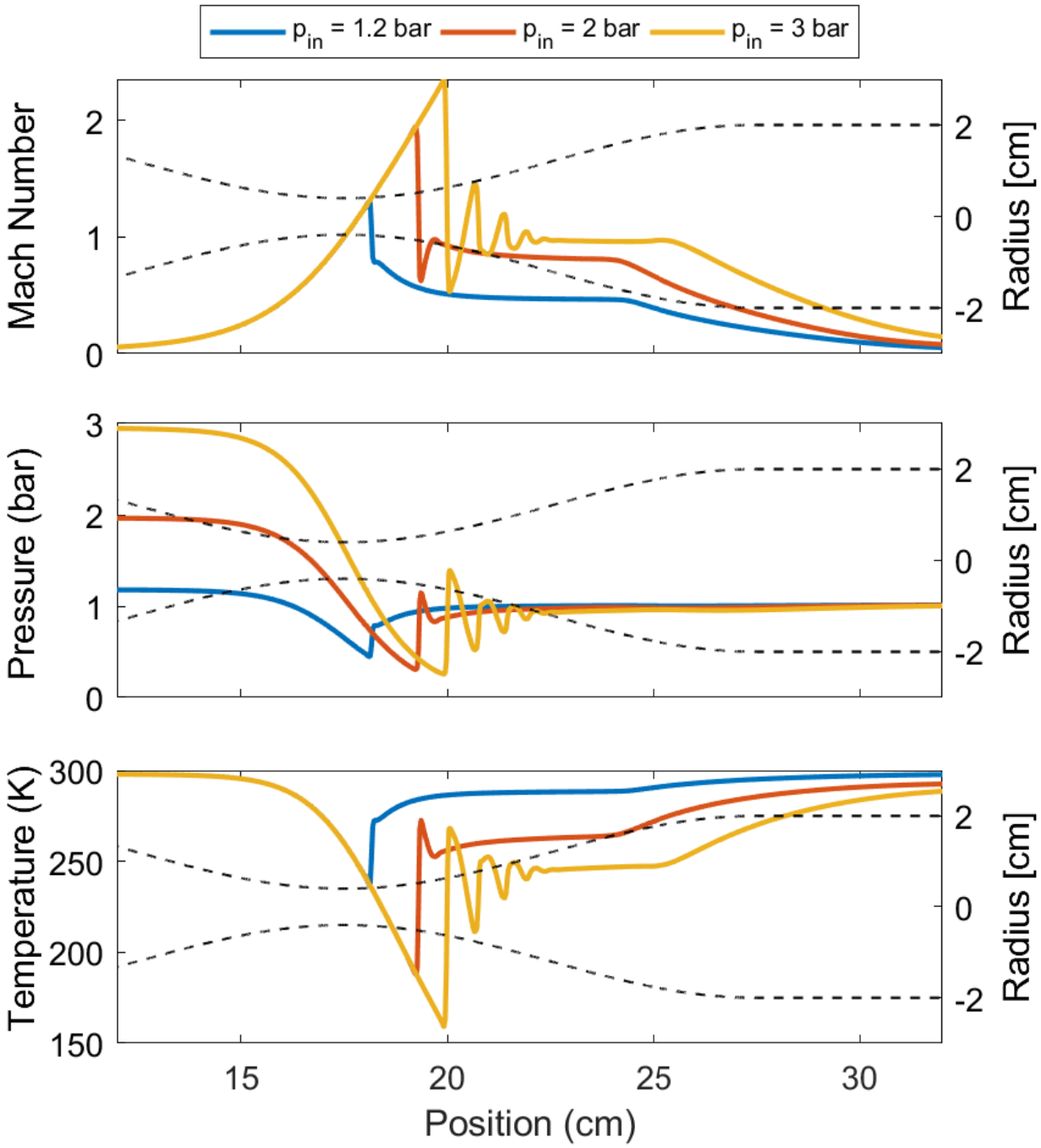

Figure S5: Mach number (top panel), pressure (middle panel) and temperature (bottom panel) as a function of position for different inlet pressures. The radius of the geometry is given in dashed lines.

6 Flow Results for Different Outlet Pressure

Figure S6 shows the evolution of the Mach number (top panel), pressure (middle panel) and temperature (bottom panel) for different outlet pressures, at an inlet pressure of 2 bar. A lower outlet pressure increases the Mach number, decreases the pressure, and decreases the temperature in the supersonic region. This makes the outlet pressure one of the main parameters to compensate for the decrease in Mach number, increase in temperature, and increase in pressure upon heat addition of the plasma.

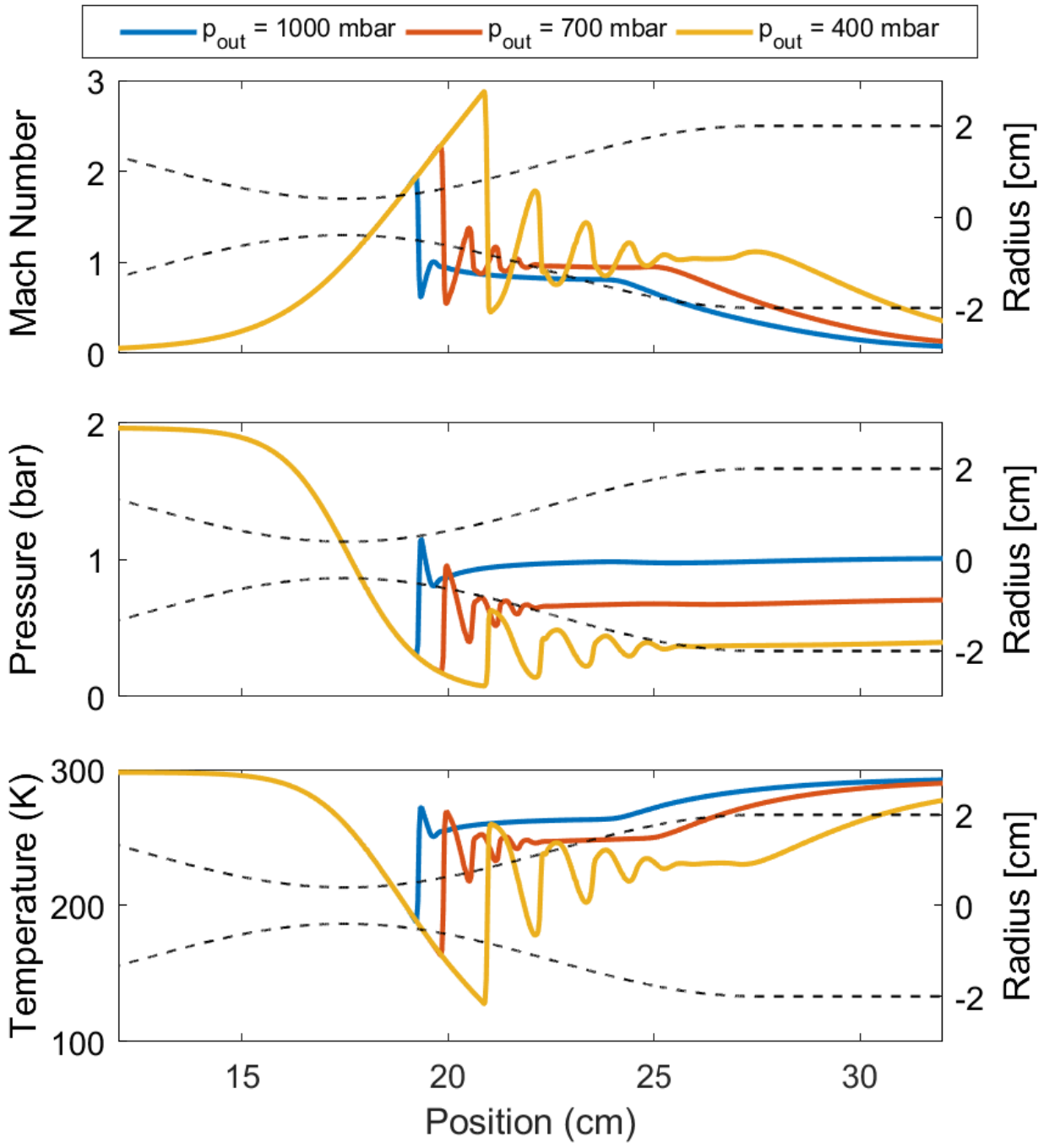

Figure S6: Mach number (top panel), pressure (middle panel) and temperature (bottom panel) as a function of position for different outlet pressures. The radius of the geometry is given in dashed lines.

7 Flow Results for Different Geometries

Figure S7 shows the evolution of the Mach number (top panel), pressure (middle panel) and temperature (bottom panel) for different values of z_1, at an inlet pressure of 2 bar and an outlet pressure of 1 bar. The supersonic region is elongated when the z_1 parameter is increased. The values of the parameters increase or decrease to the same local minima or maxima.

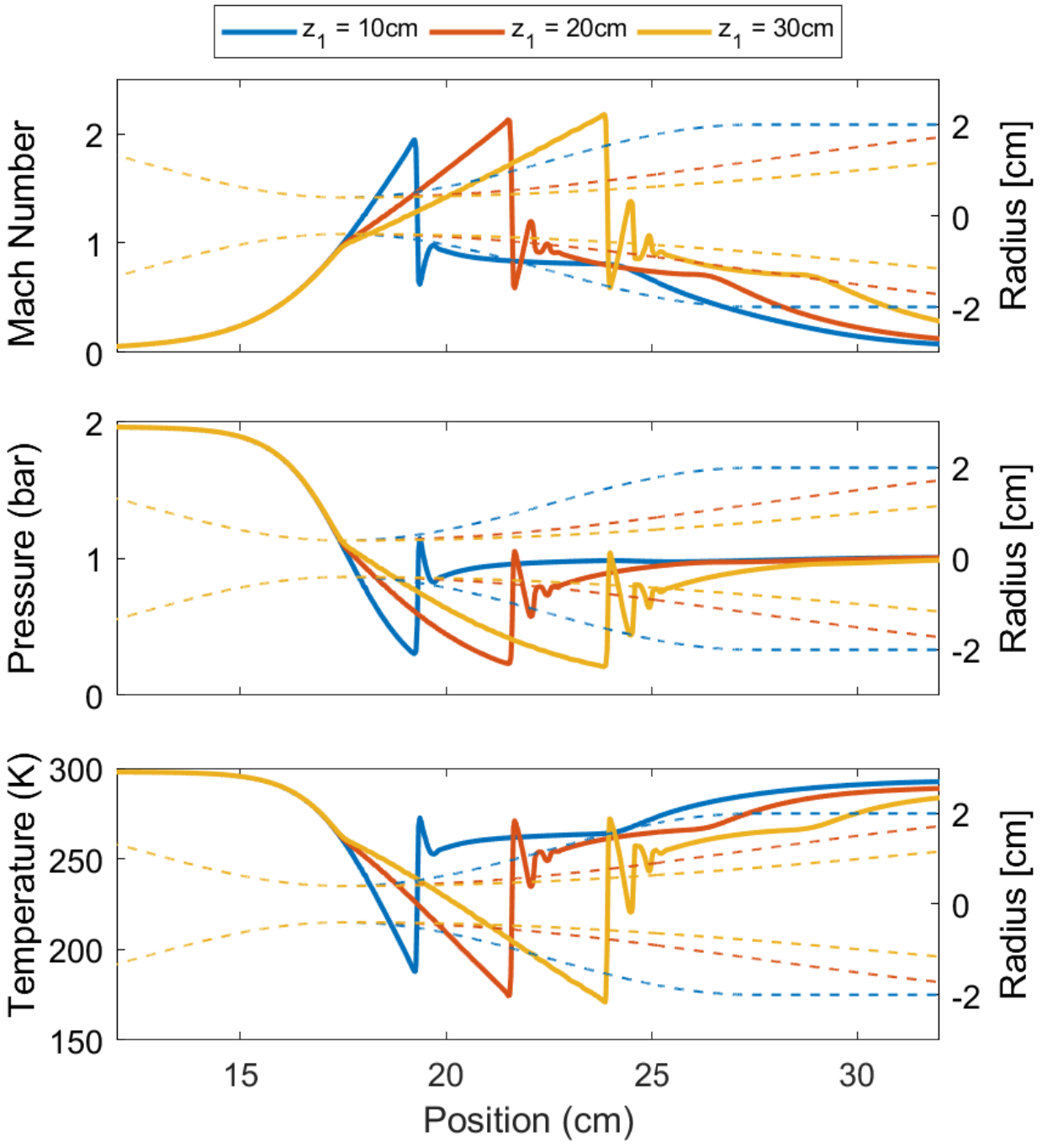

Figure S7: Mach number (top panel), pressure (middle panel) and temperature (bottom panel) as a function of position for different z_1. The radius of the geometries is given in dashed lines.

8 References

References

(S1) Phelps, A. V. Phelps Database retrieved from www.lxcat.net on September 4, 2014. http://jilawww.colorado.edu/~avp/.

(S2) Tian, C.; Vidal, C. R. Cross sections of the electron impact dissociative ionization of CO, CH_4 and C_2H_2. *Journal of Physics B: Atomic, Molecular and Optical Physics* **1998**, *31*, 895–909.

(S3) Rapp, D.; Briglia, D. D. Total Cross Sections for Ionization and Attachment in Gases by Electron Impact. II. Negative Ion Formation. *The Journal of Chemical Physics* **1965**, *43*, 1480–1489.

(S4) Land, J. E. Electron scattering cross sections for momentum transfer and inelastic excitation in carbon monoxide. *Journal of Applied Physics* **1978**, *49*, 5716–5721.

(S5) Lawton, S. A.; Phelps, A. V. Excitation of the $b^1\Sigma_g^+$ state of O_2 by low energy electrons. *The Journal of Chemical Physics* **1978**, *69*, 1055.

(S6) Weller, C. S.; Biondi, M. A. Measurements of Dissociative Recombination of CO_2^+ Ions with Electrons. *Physical Review Letters* **1967**, *19*, 59–61.

(S7) Thoenes, J.; Kurzius, S. C. *Plasma Chemistry Processes in the Closed Cycle EDL - Technical Report DRCPM-HEL-CR-79-11-VOL-1*; 1979.

(S8) Beuthe, T. G.; Chang, J.-S. Chemical Kinetic Modelling of Non-Equilibrium Ar-CO_2 Thermal Plasmas. *Japanese Journal of Applied Physics* **1997**, *36*, 4997–5002.

(S9) Mitchell, J. B. A.; Hus, H. The dissociative recombination and excitation of CO^+. *Journal of Physics B: Atomic and Molecular Physics* **1985**, *18*, 547–555.

(S10) Mcelroy, D.; Walsh, C.; Markwick, A. J.; Cordiner, M. A.; Smith, K.; Millar, T. J. The UMIST database for astrochemistry 2012. *Astronomy & Astrophysics* **2013**, *550*.

(S11) Albritton, D. Ion-neutral reaction-rate constants measured in flow reactors through 1977. *Atomic Data and Nuclear Data Tables* **1978**, *22*, 1–101.

(S12) Adams, N.; Smith, D.; Grief, D. Reactions of H_nCO^+ ions with molecules at 300 K. *International Journal of Mass Spectrometry and Ion Physics* **1978**, *26*, 405–415.

(S13) Fehsenfeld, F. C.; Ferguson, E. E. Laboratory studies of negative ion reactions with atmospheric trace constituents. *The Journal of Chemical Physics* **1974**, *61*, 3181–3193.

(S14) Mcfarland, M.; Albritton, D. L.; Fehsenfeld, F. C.; Ferguson, E. E.; Schmeltekopf, A. L. Flow-drift technique for ion mobility and ion-molecule reaction rate constant measurements. III. Negative ion reactions of O^- with CO, NO, H_2, and D_2. *Journal of Chemical Physics* **1973**, *59*, 6629–6635.

(S15) Price, D.; Moruzzi, J. Negative ion molecule reactions in CO_2 at high pressures and temperatures. *Vacuum* **1974**, *24*, 591–593.

(S16) Fehsenfeld, F. C.; Schmeltekopf, A. L.; Schiff, H. I.; Ferguson, E. E. Laboratory measurements of negative ion reactions of atmospheric interest. *Planetary and Space Science* **1967**, *15*, 373–379.

(S17) Belostotsky, S. G.; Economou, D. J.; Lopaev, D. V.; Rakhimova, T. V. Negative ion destruction by $O(^3P)$ atoms and $O_2(a^1\Delta_g)$ molecules in an oxygen plasma. *Plasma Sources Science and Technology* **2005**, *14*, 532–542.

(S18) Pack, J. L.; Phelps, A. V. Electron Attachment and Detachment. II. Mixtures of O_2 and CO_2 and of O_2 and H_2O. *The Journal of Chemical Physics* **1966**, *45*, 4316–4329.

(S19) Bortner, M. H.; Bourer, T.; Blank, C. A. *Defense Nuclear Agency Reaction Rate Handbook, Second Edition AD 763699*; 1972.

(S20) Hasted, J. B.; Smith, R. A. The Detachment of Electrons from Negative Ions. *Proceedings of the Royal Society A: Mathematical, Physical and Engineering Sciences* **1956**, *235*, 349–353.

(S21) Frommhold, L. Über verzögerte Elektronen in Elektronenlawinen, insbesondere in Sauerstoff und Luft, durch Bildung und Zerfall negativer Ionen (O^-). *Fortschritte der Physik* **1964**, *12*, 597–642.

(S22) Gudmundsson, J. T. *A critical review of the reaction set for a low pressure oxygen processing discharge RH-17-2004*; 2004.

(S23) Fridman, A. *Plasma chemistry*; Cambridge University Press: New York, 2008.

(S24) Kozák, T.; Bogaerts, A. Splitting of CO_2 by vibrational excitation in non-equilibrium plasmas: a reaction kinetics model. *Plasma Sources Science and Technology* **2014**, *23*, 045004.

(S25) Burmeister, M.; Roth, P. ARAS measurements on the thermal decomposition of CO_2 behind shock waves. *AIAA Journal* **1990**, *28*, 402–405.

(S26) Clark, T. C.; Garnett, S. H.; Kistiakowsky, G. B. Reaction of Carbon Dioxide with Atomic Oxygen and the Dissociation of Carbon Dioxide in Shock Waves. *The Journal of Chemical Physics* **1969**, *51*, 2885–2891.

(S27) Husain, D.; Young, A. N. Kinetic investigation of ground state carbon atoms, $C(2^3P_J)$. *Journal of the Chemical Society, Faraday Transactions 2* **1975**, *71*, 525.

(S28) Baldwin, R. R.; Jackson, D.; Melvin, A.; Rossiter, B. N. The second limit of hydrogen + carbon monoxide + oxygen mixtures. *International Journal of Chemical Kinetics* **1972**, *4*, 277–292.

(S29) Tsang, W.; Hampson, R. F. Chemical Kinetic Data Base for Combustion Chemistry. Part I. Methane and Related Compounds. *Journal of Physical and Chemical Reference Data* **1986**, *15*, 1087–1279.

(S30) Dean, A. J.; Davidson, D. F.; Hanson, R. K. A shock tube study of reactions of carbon atoms with hydrogen and oxygen using excimer photolysis of C_3O_2 and carbon atom atomic resonance absorption spectroscopy. *The Journal of Physical Chemistry* **1991**, *95*, 183–191.

(S31) Baulch, D. L.; Drysdale, D. D.; Duxbury, J.; Grant, S. *Evaluated Kinetic Data for High Temperature Reactions, Volume 3: Homogeneous Gas Phase Reactions of the O_2-O_3 System, the CO-O_2-H_2 System, and of the Sulphur-containing Species*; Butterworth, London, 1976.

(S32) Simpson, C. J. S. M.; Chandler, T. R. D.; Strawson, A. C. Vibrational Relaxation in CO_2 and CO_2–Ar Mixtures Studied Using a Shock Tube and a Laser–Schlieren Technique. *The Journal of Chemical Physics* **1969**, *51*, 2214–2219.

(S33) Taylor, R.; Bitterman, S. Survey of Vibrational Relaxation Data for Processes Important in the CO_2-N_2 Laser System. *Reviews of Modern Physics* **1969**, *41*, 26–47.

(S34) Blauer, J. A.; Gilmore, G. R. A survey of vibrational relaxation rate data for processes important to CO_2-N_2-H_2O infrared plume radiation. *Ultrasystems, Inc. Technical Report* **1973**, afrpl–tr–7.

(S35) Rosser, W. A.; Wood, A. D.; Gerry, E. T. Deactivation of Vibrationally Excited Carbon Dioxide (ν_3) by Collisions with Carbon Dioxide or with Nitrogen. *The Journal of Chemical Physics* **1969**, *50*, 4996–5008.

(S36) Herzfeld, K. F. Deactivation of Vibrations by Collision in the Presence of Fermi Resonance. *The Journal of Chemical Physics* **1967**, *47*, 743–752.

(S37) Capitelli, M.; Ferreira, C. M.; Gordiets, B. F.; Osipov, A. I. *Plasma kinetics in atmospheric gases*, springer s ed.; Springer Berlin Heidelberg, 2000.

(S38) Sharma, R. D. Near Resonant Vibrational Energy Transfer among Isotopes of CO_2. *Physical Review* **1969**, *177*, 102–107.

(S39) Kreutz, T. G.; O'Neill, J. A.; Flynn, G. W. Diode Laser Absorption Probe of Vibration-Vibration Energy Transfer in CO_2. *The Journal of Physical Chemistry* **1987**, *91*, 5540–5543.

(S40) DeLeon, R. L.; Rich, J. Vibrational energy exchange rates in carbon monoxide. *Chemical Physics* **1986**, *107*, 283–292.

(S41) Flament, C.; George, T.; Meister, K. A.; Tufts, J. C.; Rich, J. W.; Subramaniam, V. V.; Martin, J. P.; Piar, B.; Perrin, M. Y. Nonequilibrium vibrational kinetics of carbon monoxide at high translational mode temperatures. *Chemical Physics* **1992**, *163*, 241–262.

(S42) Matsuo, K.; Miyazato, Y.; Kim, H.-d. Shock train and pseudo-shock phenomena in internal gas flows. **1999**, *35*, 33–100.